PCCP

A Strategy for Boosting Thermoelectric Performance of Famatinite Cu_3SbS_4

Journal:	*Physical Chemistry Chemical Physics*
Manuscript ID	CP-ART-11-2019-006233.R1
Article Type:	Paper
Date Submitted by the Author:	20-Dec-2019
Complete List of Authors:	Tanishita, Taiki; Kyushu University Suekuni, Koichiro; Kyushu University Nishiate, Hirotaka; National Institute of Advanced Industrial Science and Technology Tsukuba Center Tsukuba Central Lee, Chul-Ho; National Institute of Advanced Industrial Science and Technology Tsukuba Center Tsukuba Central Ohtaki, Michitaka; Kyushu University

PCCP

ARTICLE

A Strategy for Boosting Thermoelectric Performance of Famatinite Cu_3SbS_4

Received 00th January 20xx,
Accepted 00th January 20xx

DOI: 10.1039/x0xx00000x

Taiki Tanishita, [a] Koichiro Suekuni, [*a,b] Hirotaka Nishiate, [c] Chul-Ho Lee, [c] Michitaka Ohtaki, [a,b]

Famatinite Cu_3SbS_4 has attracted attention for its potential application in thermoelectric (TE) contexts. In this work, we report the impacts of co-substituting Ge and P for Sb on TE properties. Melting and heat treatment methods were adopted to synthesize samples of $Cu_3Sb_{1-x-y}Ge_xP_yS_4$ ($x \le 0.4$, $y \le 0.3$). In this system, Ge functioned as an acceptor for doping a hole to the valence band, which led to enhancement of the TE power factor. Contrastingly, P barely altered electronic structure. Furthermore, both Ge and P acted as point defects, which effectively decreased lattice thermal conductivity. The combined effects of the co-substitution gave rise to an enhanced dimensionless figure of merit, *ZT*, of 0.67 at 673 K.

1 INTRODUCTION

Direct conversion from thermal energy into electrical energy in solids based on the Seebeck effect is referred to as thermoelectric (TE) conversion. This conversion technique has attracted increasing attention due to its potential applications, for example, in waste heat recovery power generators.[1] In this instance, output power is dependent on output voltage and the (internal) electrical resistance of a solid-state device. The electric potential difference, ΔV, is proportional across the device to the temperature difference, ΔT as $\Delta V = S\Delta T$, where S is the Seebeck coefficient. For maintaining sufficient ΔT and hence a high level of ΔV, low thermal conductance is a requisite characteristic for a TE conversion device. Therefore, the materials used in such a device are required to have a high S; a low electrical resistivity, ρ; and a low thermal conductivity, κ, for implementing efficient TE conversion. In fact, the material's properties are associated with the conversion efficiency through the dimensionless figure of merit $ZT = S^2T\rho^{-1}\kappa^{-1}$, where $S^2\rho^{-1}$ is recognized as a power factor.

In addition to high performance (high ZT), earth-abundant and less toxic characteristics are desired for TE materials realizing large-scale and cost-effective applications. Over the past decade, Cu–S-based materials, which fulfill the above requirements, have emerged as promising candidates for p-type TE materials.[2–20] Examples include famatinite (Cu_3SbS_4)-based materials.[12–16] Cu_3SbS_4 has a zinc-blende (ZnS)-derivative tetragonal structure (*I*-42*m*), which can be obtained by doubling the ZnS unit cell and replacing the Zn atoms with Cu and Sb atoms in an ordered manner.[21,22] The Cu and Sb atoms occupy inequivalent crystallographic sites and are tetrahedrally coordinated by S atoms. The formal valences of these atoms can be expressed as $Cu^{+}{}_3Sb^{5+}S^{2-}{}_4$. Cu_3SbS_4 is a semiconductor with an energy gap of ~1 eV between the valence band and the conduction band.[13] The top of the valence band is composed primarily of Cu 3d and S 3p orbitals, whereas the lowest conduction band comprises Sb 5s and S 3p orbitals.[13,23] Here, the former characteristic indicates that the corner-shared CuS_4 tetrahedron network governs the p-type conduction of Cu_3SbS_4. Three-fold band degeneracy at the top of the valence band results in large density of states, with an effective mass of $m^* = 3.0–3.6m_0$, where m_0 is the electron rest mass.[13–15] Therefore, a high S ($\propto m^*p^{-2/3}$) can be maintained even when the hole carrier concentration, p, reaches as high as 10^{21} cm^{-3}. Indeed, for a hole-doped Cu_3SbS_4, the combination of a low ρ and a relatively high S gives rise to a high $S^2\rho^{-1}$ of ~1.3 mW K^{-2} m^{-1} at 623 K.[14,15] An aliovalent substitution of Ge^{4+}/Sn^{4+} for Sb^{5+} was adopted for dope holes.[12–16] Despite superior electronic properties, Cu_3SbS_4 exhibited relatively high κ for TE materials, where the lattice component, κ_{lat}, was as high as ~1 W K^{-1} m^{-1} at 623 K.[13,14] This may have been due to a feature of the crystal structure, e.g., its small primitive cell volume.[24] One means by which κ_{lat} can be decreased is through the introduction of phonon scatterers (point defects) by substituting Se for S,[25,26] and another approach is through the enhancement of phonon grain-boundary scattering.[14,15] The reduction in κ_{lat} led to the enhancement of ZT to 0.7 at 623 K for $Cu_3Sb_{1-x}Sn_xS_4$,[14,16] to 0.6 at 623 K for $Cu_3Sb_{1-x}Ge_xS_4$,[15] and to 0.8 at 673 K for $Cu_3Sb_{1-x}Ge_xS_{4-z}Se_z$.[26] The highest ZT was obtained for the Se substituted samples. However, Se is prevent from being utilized in large-scale applications due to the toxicity.

In this work, we propose an alternative strategy to boost ZT for Cu_3SbS_4 without Se, i.e., co-substitution of Ge and P for Sb. In the co-substituted system, $Cu_3Sb_{1-x-y}Ge_xP_yS_4$, Ge functioned

[a] Department of Applied Science for Electronics and Materials, Interdisciplinary Graduate School of Engineering Sciences, Kyushu University, Kasuga, Fukuoka 816-8580, Japan
[b] Transdisciplinary Research and Education Center for Green Technologies, Kyushu University, Kasuga, Fukuoka 816-8580, Japan
[c] Research Institute for Energy Conservation, National Institute of Advanced Industrial Science and Technology (AIST), Tsukuba, Ibaraki 305-8568, Japan

†Electronic Supplementary Information (ESI) available. See DOI: 10.1039/x0xx00000x

as an acceptor for doping a hole, leading to enhanced $S^2\rho^{-1}$. Furthermore, Ge and P functioned as point defects responsible for phonon scattering, leading to decreased κ_{lat}. As a result, ZT = 0.67 at 673 K was achieved for $Cu_3Sb_{1-x-y}Ge_xP_yS_4$ with x = 0.1, y = 0.15.

2 EXPERIMENTAL PROCEDURE

We prepared the co-substituted samples of $Cu_3Sb_{1-x-y}Ge_xP_yS_4$ (x = 0.05, 0.1, 0.2, 0.3, 0.4, y = 0.05, 0.1, 0.15, 0.3) by melting the constituent elements, followed by exposure to heat treatment. The elements were sealed in an evacuated quartz tube and heated at 1073 K over a period of 24 h. The obtained ingot was clashed into powder and molded into a pellet. The pellet was sealed in an evacuated quartz tube and then heated at 873 K over a period of 50 h to improve homogeneity. The sample was clashed again and loaded into a graphite die, which was heated to 873 K under uniaxial pressure of 50 MPa in a flowing N_2 atmosphere. Hot-press sintering was effected in a furnace PLASMAN CPS-KIT-03121 (S.S. Alloy). For the synthesis of non-substituted ($x = y = 0$), Ge-substituted (x = 0.1, y = 0), and P-substituted (x = 0, y = 0.15) samples, a reported procedure[25] was partially followed to suppress the formation of impurity phases. The constituted elements were heated at 1073 K in an evacuated quartz tube, cooled to 873 K, and then quenched in water. The quartz tube was subsequently heated at 623 K over a period of 48 h. Hot-press sintering was performed at 823 K or 873 K. The relative density of all sintered samples was as high as ≥ 98%.

Powder X-ray diffraction (XRD) data were collected in the range 10° ≤ 2ϑ ≤ 100° using a MiniFlex diffractometer (Rigaku) equipped with a Cu Kα radiation source. Rietveld refinement of the pattern was effected to evaluate the lattice parameters, a and c, of the famatinite phase, using the RIETAN FP software package.[27] Scanning electron microscopy (SEM) and energy-dispersive spectroscopy (EDS) were performed using a JCM-6000Plus NeoScope (JEOL) microscope.

ρ and S were simultaneously measured using a four-probe DC method and a temperature differential method, respectively, using a ZEM-3 (ADVANCE RIKO) measurement system under a low-pressure He atmosphere, at 300 K–673 K. Thermal diffusivity α and specific heat C_P at 300 K–673 K were measured simultaneously using an LFA-457 MicroFlash® thermal analyzer (Netzsch), using a laser-flash method in a flowing Ar atmosphere. The absolute values of C_P were derived from a comparison between the measured values, with C_P values measured for a standard sample of Pyroceram 9606 (Netzsch). These data were used to calculate the thermal conductivity using the relation $\kappa = \alpha C_P d_s$, where d_s was the sample density estimated from the dimensions and weight of the sample. It should be noted that the obtained C_p values of 0.43–0.55 J g^{-1} K^{-1} at temperatures between 300 and 673 K corresponded to molar C_p values of 189–229 J mol^{-1} K^{-1} per $Cu_3Sb_{1-x-y}Ge_xP_yS_4$. The latter molar values agreed to a reasonable degree with the Dulong–Petit value of 200 J mol^{-1} K^{-1}. We confirmed the reproducibility of the ρ, S, α, and C_P data upon both heating and cooling in the range of 300–673 K, except for ρ and S data in the

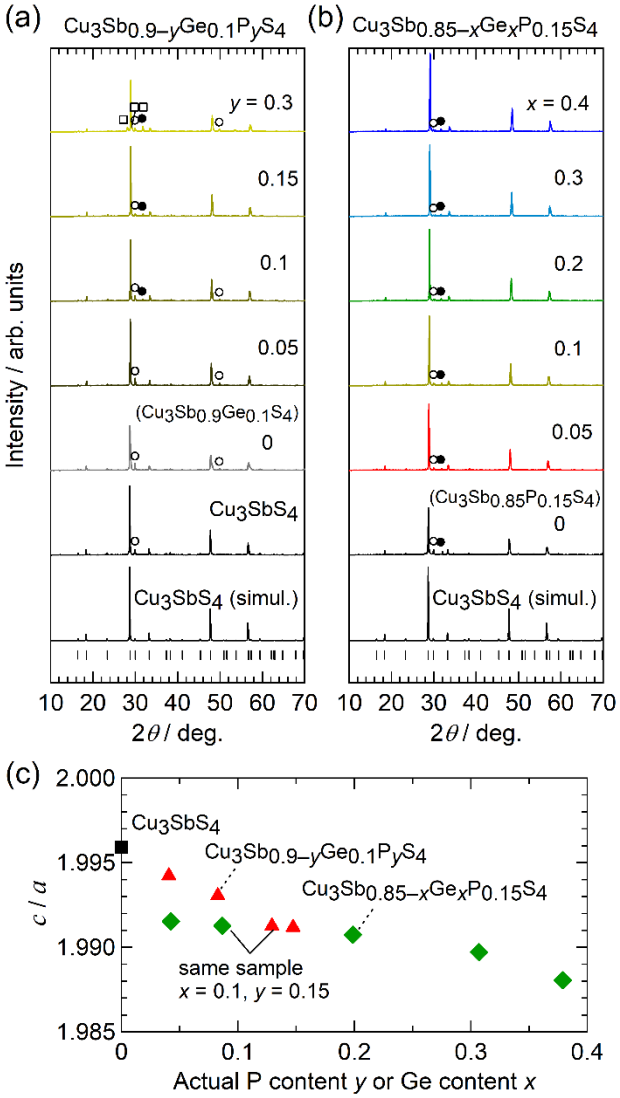

Fig. 1. Powder X-ray diffraction patterns for the samples of (a) Cu_3SbS_4 and $Cu_3Sb_{0.9-y}Ge_{0.1}P_yS_4$ (y = 0–0.3) and (b) $Cu_3Sb_{0.85-x}Ge_xP_{0.15}S_4$ (x = 0–0.4). The simulated pattern based on the famatinite (Cu_3SbS_4) structure is shown at the bottom in (a) and (b). Peaks denoted by open circle, closed circle, and open square represent tetrahedrite $Cu_{12}Sb_4S_{13}$, argyrodite $Cu_{7-8}(Ge, P)S_6$, and enargite Cu_3PS_4, respectively. (c) Ratio of lattice parameters, c/a, with respect to the actual P content, y, for $Cu_3Sb_{0.9-y}Ge_{0.1}P_yS_4$, and to the actual Ge content, x, for $Cu_3Sb_{0.85-x}Ge_xP_{0.15}S_4$. The c/a value and chemical composition are also listed in Table S1 in the ESI†.

$x = y = 0$ and $x = 0$, y =0.15 samples. For the non-substituted sample, ρ and S showed irreversible drops above 600 K (Fig. S1 in the ESI†), inferring that degradation of the sample had occurred in the low-pressure environment. Hall effect measurements were performed using a four-probe DC method on a laboratory-built system, with a permanent magnet generating a magnetic field, B, of 0.62 T at 300 K. We calculated carrier concentration p as $R_H^{-1}e^{-1}$ on the basis of the single-carrier model and Hall mobility of μ_H as $R_H\rho^{-1}$, where R_H was the Hall coefficient and e was elementary charge.

3 RESULTS AND DISCUSSION

The samples of $Cu_3Sb_{1-x-y}Ge_xP_yS_4$ were characterized by analyzing XRD, SEM, and EDS data. For all samples, peak

positions and the intensities of XRD patterns agreed to a reasonable degree with those of a simulated pattern based on the famatinite (Cu_3SbS_4) structure (Figs. 1(a), 1(b)).[21] Additional small peaks were indexed to the tetrahedrite $Cu_{12}Sb_4S_{13}$ (*I*-43*m*), argyrodite $Cu_{7-8}(P,Ge)S_6$ ($P2_13$), and enargite Cu_3PS_4 ($Pmn2_1$) phases, which were also observed from SEM/EDS (backscattered electron images are shown in Fig. S2 in the ESI†). To evaluate the chemical composition of the famatinite phase, EDS was performed across 15 points and the data were averaged (Table S1 in the ESI†). Here, the composition was calculated by assuming the sum of the composition of cation (Cu, Sb, Ge, and P) as being 4.

For the non-substituted sample of $x = y = 0$ (Fig. 1(a)), Rietveld refinement of the XRD pattern yielded $a = 5.386$ Å and $c = 10.751$ Å for the famatinite phase, and EDS showed the actual composition as being close to that of the stoichiometric composition (Table S1 in the ESI†). The Ge-substituted sample of $x = 0.1$, $y = 0$ showed broad XRD peaks in the famatinite phase (Fig. 1(a)), which was consistent with the separation into Ge-poor and Ge-rich matrices observed from EDS. The P-substituted sample of $x = 0$, $y = 0.15$ was composed of a single famatinite phase (Fig. 1(b)), though the actual P content, 0.04, was one third of the starting composition (Table S1 in the ESI†).

We then characterized the co-substituted series with $x = 0.1$ ($Cu_3Sb_{0.9-y}Ge_{0.1}P_yS_4$, Fig. 1(a)). The samples $y = 0.05$–0.3 comprised single famatinite phases, the *a* and *c* of which decreased as *y* increased. This result can be attributed to the smaller ionic radius of P^{5+} (0.17 Å) compared with that of Sb^{5+} (0.565 Å).[14,28] Actual compositions agreed with starting compositions for the samples of $y \le 0.15$. On the other hand, the sample indicating $y = 0.3$ had a poor P composition of 0.15 (Table S1 in the ESI†) and exhibited an impurity phase with P, Cu_3PS_4 (Fig. 1; Fig. S2 in the ESI†). Therefore, the solubility limit of P in the series $Cu_3Sb_{0.9-y}Ge_{0.1}P_yS_4$ may have been $y \sim 0.15$. This value was higher than the actual P content, 0.04, in the aforementioned P-only substituted sample of $x = 0$, $y = 0.15$.

Following on, another co-substituted series with $y = 0.15$ ($Cu_3Sb_{0.85-x}Ge_xP_{0.15}S_4$, Fig. 1(b)) was prepared. The values of *a* and *c* decreased as *x* increased, from 0.05 to 0.4 (Table S1 in the ESI†), which resulted from the smaller ionic radius of Ge^{4+} (0.39 Å) compared with that of Sb^{5+} (0.565 Å).[14,28] Actual compositions agreed with starting compositions for the samples of $x = 0.05$–0.3 (Table S1 in the ESI†).

The aforementioned results indicated reluctance to solely incorporate P into the famatinite structure and enhancement of the solubility of P to $y \sim 0.15$ in $Cu_3Sb_{1-x-y}Ge_xP_yS_4$ by the Ge substitution. It was reported that Cu_3SbS_4 and Cu_3PS_4 did not form a solid solution series, whereas Cu_3SbS_4 and Cu_3AsS_4 formed a $Cu_3Sb_{1-y}As_yS_4$ series with a famatinite structure up to $y = 0.7$.[22] The solubility of P/As to Sb was likely subject to the magnitude of mismatch in the ionic radius between P^{5+} (0.17 Å)/As^{5+} (0.335 Å) and Sb^{5+} (0.565 Å).[14,28] It was anticipated that the substitution of small P for large Sb would introduce a significant distortion in the famatinite structure; therefore, substitution was avoided for Cu_3SbS_4. In this context, Ge^{4+} may be allowed to participate in the famatinite structure, because the ionic radius of Ge^{4+} (0.39 Å) is similar to that of As^{5+}. We

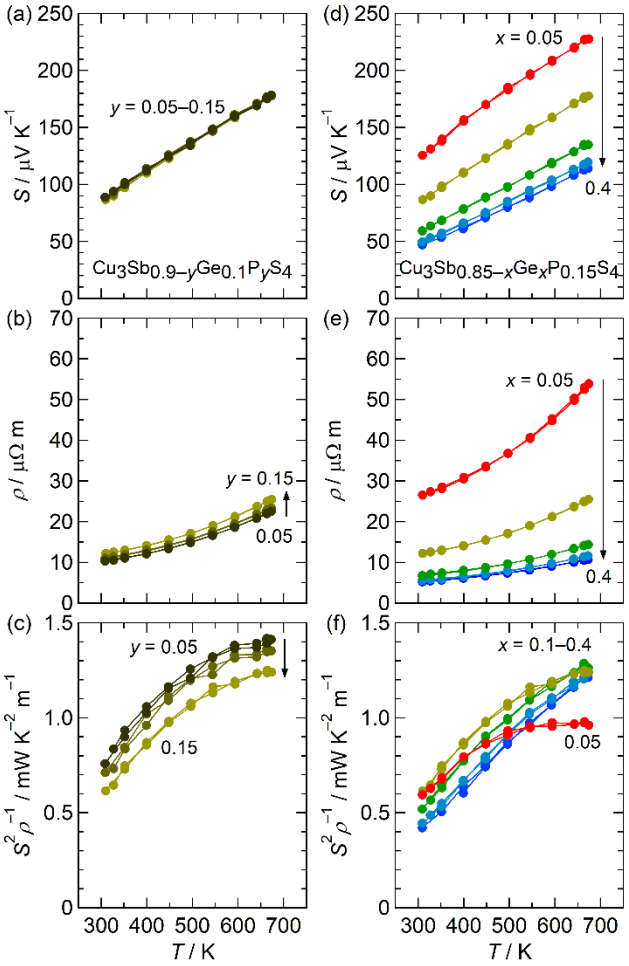

Fig. 2. (a),(d) Seebeck coefficient, *S*; (b),(e) electrical resistivity, *ρ*; (c),(f) power factor, $S^2\rho^{-1}$, for the samples $Cu_3Sb_{0.9-y}Ge_{0.1}P_yS_4$ ($y = 0.05$, 0.1, 0.15) and $Cu_3Sb_{0.85-x}Ge_xP_{0.15}S_4$ ($x = 0.05$, 0.1, 0.2, 0.3 0.4). (a)–(f) Figures show data upon both heating and cooling, which are overlapping.

conjectured that the reception of P in the co-substituted system ($Cu_3Sb_{1-x-y}Ge_xP_yS_4$) can be attributed to the reduction in lattice parameters and/or to the local distortion/relaxation of structure, effected by the Ge substitution.

Degree of structural distortion can be measured by deviation of *c*/*a* from the ideal value of 2.[22] It was reported that the substitution of As for Sb as $Cu_3Sb_{1-y}As_yS_4$ linearly decreased *c*/*a* from 1.997 ($y = 0$) to 1.981 ($y = 0.7$). In our samples $Cu_3Sb_{1-x-y}Ge_xP_yS_4$, the *c*/*a* ratio also decreased from 1.996 to 1.988 alongside increasing *x* and *y* (Fig. 1(c), Table S1 in the ESI†). The reduction in *c*/*a* by the P substitution ($Cu_3Sb_{0.9-y}Ge_{0.1}P_yS_4$) was pronounced, compared with that by the Ge substitution ($Cu_3Sb_{0.85-x}Ge_xP_{0.15}S_4$), indicating that the P substitution resulted in a significant structure distortion.

Next, the electronic properties of $Cu_3Sb_{1-x-y}Ge_xP_yS_4$ (Fig. 2) are addressed, excluding the Ge-substituted sample of $x = 0.1$, $y = 0$ with the inhomogeneous famatinite phase, and for the P-substituted sample of $x = 0$, $y = 0.15$ and the sample of $x = 0.1$, $y = 0.3$ with the P-poor compositions described above. The non-substituted sample of $x = y = 0$ exhibited $\rho = 3.5 \times 10^{-2}$ Ω m and $S = 537$ μV K^{-1} at 300 K (Fig. S1 in the ESI†). These high values arose from a low hole carrier concentration of 1.5×10^{17} cm^{-3}.

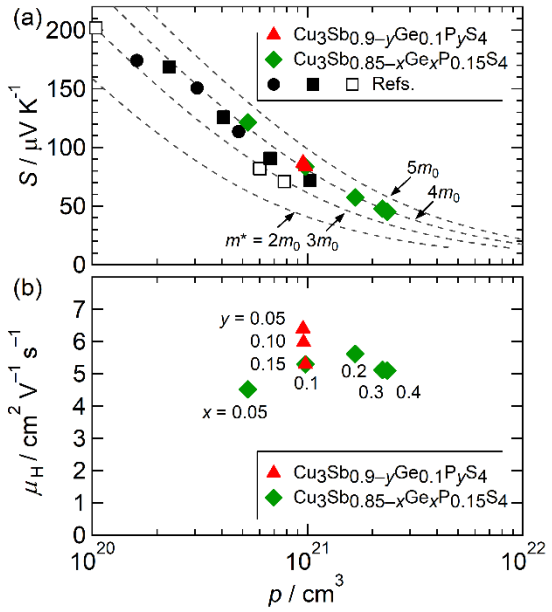

Fig. 3. (a) The relationship between the Seebeck coefficient, S, and the hole carrier concentration, p, for $Cu_3Sb_{1-x-y}Ge_xP_yS_4$ (closed diamonds and triangles), $Cu_3Sb_{1-x}Ge_xS_4$ (closed circles[15]), and $Cu_3Sb_{1-x}Sn_xS_4$ (closed squares[14], open squares[13]). Theoretical curves (dashed line) based on the effective mass of hole m^* of $2m_0$, $3m_0$, $4m_0$, and $5m_0$ are shown. Details regarding the calculations of S and p are described in the text. (b) Hall mobility μ_H with respect to the p for $Cu_3Sb_{1-x-y}Ge_xP_yS_4$.

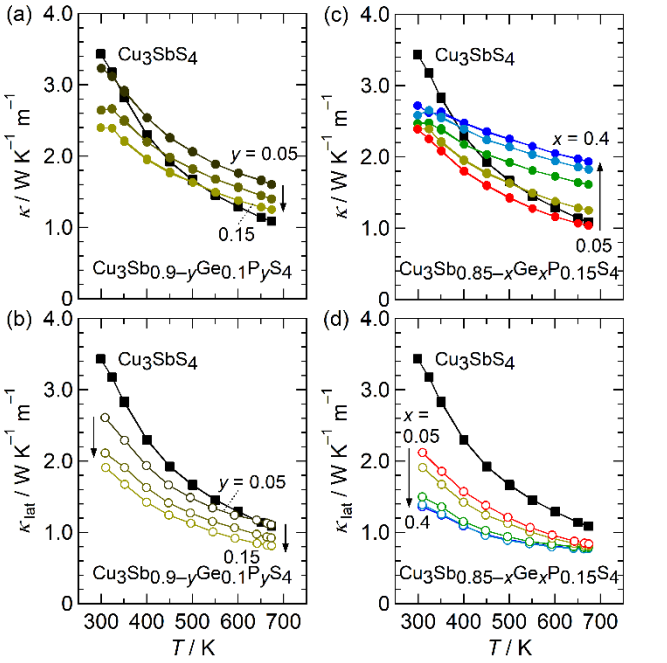

Fig. 4. (a),(c) Thermal conductivity, κ; (b),(e) the lattice component, κ_{lat}, for the samples of $Cu_3Sb_{0.9-y}Ge_{0.1}P_yS_4$ (y = 0.05, 0.1, 0.15) and $Cu_3Sb_{0.85-x}Ge_xP_{0.15}S_4$ (x = 0.05, 0.1, 0.2, 0.3, 0.4). In all figures, κ for Cu_3SbS_4 is shown for comparison. (a), (c) Figures show data upon both heating and cooling, which are overlapping.

In contrast, the samples $Cu_3Sb_{0.9-y}Ge_{0.1}P_yS_4$ (y = 0.05–0.15) and $Cu_3Sb_{0.85-x}Ge_xP_{0.15}S_4$ (x = 0.05–0.4) showed a much lower ρ and S (Fig. 2). The positive sign of S indicated that dominant charge carriers were holes, and the positive slopes (metallic behavior) of ρ and S, with respect to temperature, proved that Fermi level was situated in the valence band.

The values of S agreed among three samples of $Cu_3Sb_{0.9-y}Ge_{0.1}P_yS_4$ (Fig. 2(a)), which was consistent with equal p values of 1.0×10^{21} cm^{-3} (Fig. 3(a)). These results can be attributed to the same amount of hole dopant (Ge) being present in the samples and indicate negligible modification of the electronic structure near the Fermi level by the P (isovalent) substitution. Furthermore, the agreements in S and n, regardless of the different amounts of impurity phases, suggest that the impurity phases barely/equally affected the properties of $Cu_3Sb_{0.9-y}Ge_{0.1}P_yS_4$. On the other hand, the value of ρ slightly increased alongside an increasing y (Fig. 2(b)), which was associated with a decrease in μ_H from 6.4 to 5.3 cm^2 V^{-1} s^{-1} (Fig. 3(b)). The reduced μ_H may result from distortion of the Cu–S network induced by the P substitution, as suggested by the large reduction in c/a (Fig. 1(c); Table S1 in the ESI†). Further theoretical investigation of the relationship between the distortion of the Cu–S network and carrier relaxation time are required. The $S^2\rho^{-1}$ for the sample y = 0.05 increased with increasing temperature and reached as high as 1.4 mW K^{-2} m^{-1} at 673 K (Fig. 2(c)). However, the value of $S^2\rho^{-1}$ decreased alongside an increasing y, which remained higher than 1.25 mW K^{-2} m^{-1}. For the samples $Cu_3Sb_{0.85-x}Ge_xP_{0.15}S_4$, the values of ρ and S decreased alongside an increasing x, which resulted from the increase in p from 0.5×10^{21} (x = 0.05) to 2.3×10^{21} cm^{-3} (x = 0.4) (Figs. 2(d), 2(e), 3(a)). Here, μ_H was roughly constant at ~5 cm^2 V^{-1} s^{-1} with respect to Ge content (Fig. 3(b)). As a result, $S^2\rho^{-1}$ was kept at a high value of 1.2–1.3 mW K^{-2} m^{-1} at 673 K, except for the sample x = 0.05 (Fig. 2(f)).

In order to gain insight into the electronic structure of $Cu_3Sb_{1-x-y}Ge_xP_yS_4$, we investigated the relationship between S and p by comparing the experimental data with the theoretical data. The theoretical p and S values were calculated using equations $p = (4/\pi^{1/2})(2\pi m^* k_B T/h^2)^{3/2} F_{1/2}(\eta)$ and $S = (k_B/e)(2F_1(\eta)/F_0(\eta) - \eta)$, respectively, where k_B was the Boltzmann constant, h was Planck's constant, $F_n(\eta)$ was the Fermi integral, and η was reduced chemical potential.[29] It should be noted that these equations were based on a single parabolic band, and the carrier relaxation time was limited by acoustic phonon scattering. The experimental data fell on the curves of m^* = 3–4m_0 for our $Cu_3Sb_{1-x-y}Ge_xP_yS_4$, similar to the reported $Cu_3Sb_{1-x}(Ge/Sn)_xS_4$ samples.[13–15] Thus, the P substitution up to y = 0.15 and the Ge substitution up to x = 0.4 were found to have barely changed the m^*.

Next, we focused on the effects of the Ge and P substitution on κ and κ_{lat}. For the non-substituted semiconducting sample $x = y = 0$, $\kappa \sim \kappa_{lat}$ was 3.4 W K^{-1} m^{-1} at 300 K and monotonically decreased to 1.0 W K^{-1} m^{-1} at 673 K (Fig. 4). The temperature dependence resulted from the Umklapp scattering of phonons. Compared with the non-substituted sample, the value of κ decreased at 300 K and, contrastingly, increased at 673 K for the co-substituted samples of $Cu_3Sb_{0.9-y}Ge_{0.1}P_yS_4$ and $Cu_3Sb_{0.85-x}Ge_xP_{0.15}S_4$ (Figs. 4(a), 4(c)). The rise in κ at 673 K originated from an increase in the electronic component of thermal conductivity κ_{ele}. We estimated κ_{ele} using the Wiedemann–Franz law, $LT\rho^{-1}$, where the Lorenz number, L, was

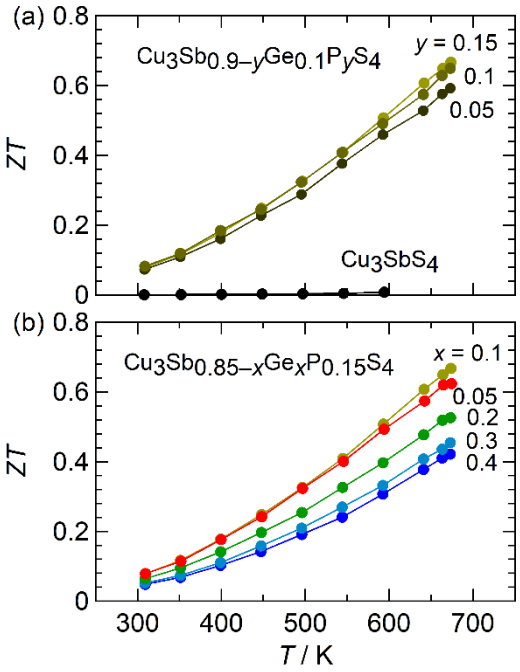

Fig. 5. Dimensionless figure of merit *ZT* for famatinites: (a) $Cu_3Sb_{0.9-y}Ge_{0.1}P_yS_4$ (y = 0.05–0.15) and Cu_3SbS_4, (b) $Cu_3Sb_{0.85-x}Ge_xP_{0.15}S_4$ (x = 0.05–0.4).

calculated by using the equation $L = (k_B/e)^2(3F_0(\eta)F_2(\eta) - 4F_1(\eta)^2)/F_0(\eta)^2$.[29] The L values were 1.58–2.24 × 10^{-8} W Ω K^{-2} for the samples, except for x = 0, y = 0. We then subtracted κ_{ele} from κ to obtain κ_{lat}. The values of κ_{lat} for the samples of $Cu_3Sb_{0.9-y}Ge_{0.1}P_yS_4$ and $Cu_3Sb_{0.85-x}Ge_xP_{0.15}S_4$ decreased alongside an increasing y and x, respectively (Figs. 4(b), 4(d)). As a result of the co-substitution, κ_{lat} was reduced from 3.4 to 1.4 W K^{-1} m^{-1} at 300 K and from 1.1 to 0.8 W K^{-1} m^{-1} at 673 K. The reduction in κ_{lat} indicated that both Ge and P, substituted for Sb, functioned as point defects that induced mass/strain fluctuation, responsible for phonon scattering. The reduction in κ_{lat} by the P substitution manifested throughout the entire temperature range (Fig. 4(b)), whereas the reduction by Ge substitution was pronounced at the low-temperature region (Fig. 4(d)). The significant suppression of κ_{lat} at 673 K was likely the result of the prominent distortion of the crystal structure, induced by the P substitution (Fig. 1(c)). The lowest value of κ_{lat} (0.8 W K^{-1} m^{-1}) in this instance is greater than the κ_{lat} value of 0.6 W K^{-1} m^{-1} for a Se-substituted sample.[26] On the other hand, the lowest value is comparable with the κ_{lat} value for a sample synthesized by mechanical alloying, followed by spark plasma sintering, which exhibited small-sized grains connected by twinning boundaries.[14–16]

As described above, the P substitution for Sb decreased κ_{lat} while keeping the electronic structure intact, whereas the Ge substitution doped holes to the valence band and decreased κ_{lat}. The combined substitution effect led to the enhancement of *ZT* to 0.4–0.7 (Fig. 5). For the $Cu_3Sb_{0.9-y}Ge_{0.1}P_yS_4$ (y = 0.05–0.15) series, *ZT* at 673 K increased from 0.6 to 0.7 alongside an increasing y (Fig. 5a), which was primarily the result of a reduction in κ_{lat}. For the $Cu_3Sb_{0.85-x}Ge_xP_{0.15}S_4$ (x = 0.05–0.4) series, *ZT* was maximized at x = 0.1 and decreased alongside an increasing x at $x \geq 0.2$ (Fig. 5b), the latter of which resulted from an increase in κ_{ele}.

4 Conclusions

In summary, we investigated the crystal structure and TE properties of famatinites $Cu_3Sb_{1-x-y}Ge_xP_yS_4$. The solubility of P to Sb was enhanced to 0.15 when Ge partly replaced Sb. The Ge (aliovalent) substitution increased p, leading to enhanced $S^2\rho^{-1}$. The P (isovalent) substitution barely modified the electronic structure and hardly altered the p. Ge and P substituted for Sb both functioned as point defects responsible for phonon scattering. Specifically, the substitution of P resulted in the drastic suppression of κ_{lat} at 673 K. These impacts of the co-substitution of Ge and P on TE properties led to *ZT* of 0.67 at 673 K for the sample of x = 0.1, y = 0.15. Such a co-substitution strategy will likely be useful for boosting TE performance for Cu–S-based materials.

Conflicts of interest

There are no conflicts of interest to declare

Acknowledgements

We are grateful to H. Usui for fruitful discussion on the electronic structure. This work was supported financially by grants from CREST JST under Grant No. JPMJCR16Q6, grants from the International Joint Research Program for Innovative Energy Technology funded by METI, and JSPS KAKENHI under Grant No. JP17H04951 (K.S.), Japan.

References

1 L. E. Bell, *Science*, 2008, **321**, 1457.
2 K. Suekuni and T. Takabatake, *APL Mater.*, 2016, **4**, 104503.
3 A. V. Powell, *J. Appl. Phys.*, 2019, **126**, 100901.
4 M. L. Liu, F. Q. Huang, L. D. Chen, and I. W. Chen, *Appl. Phys. Lett.*, 2009, **94**, 202103.
5 Z. H. Ge, B. P. Zhang, Y. X. Chen, Z. X. Yu, Y. Liu, and J. F. Li, *Chem. Commun.*, 2011, **47**, 12697.
6 Y. He, T. Day, T. Zhang, H. Liu, X. Shi, L. Chen, G. J. Snyder, *Adv. Mater.*, 2014, **26**, 3974.
7 X. Lu, D. T. Morelli, Y. Xia, F. Zhou, V. Ozolins, H. Chi, X. Zhou, and C. Uher, *Adv. Energy Mater.*, 2013, **3**, 342.
8 K. Suekuni, K. Tsuruta, M. Kunii, H. Nishiate, E. Nishibori, S. Maki, M. Ohta, A. Yamamoto, and M. Koyano, *J. Appl. Phys.*, 2013, **113**, 043712.
9 K. Suekuni, F. S. Kim, H. Nishiate, M. Ohta, H. I. Tanaka, and T. Takabatake, *Appl. Phys. Lett.*, 2014, **105**, 132107.
10 Y. Kikuchi, Y. Bouyrie, M. Ohta, K. Suekuni, M. Aihara and T. Takabatake, *J. Mater. Chem. A*, 2016, **4**, 15207.
11 V. Pavan Kumar, A. R. Supka, P. Lemoine, O. I. Lebedev, B. Raveau, K. Suekuni, V. Nassif, R. Al Rahal Al Orabi, M. Fornari, and E. Guilmeau, *Adv. Energy. Mater.*, 2018, **9**, 1803249.
12 A. Suzumura, M. Watanabe, N. Nagasako, and R. Asahi, *J. Electron. Mater.*, 2014, **43**, 2356.
13 Y. Goto, Y. Sakai, Y. Kamihara, and M. Matoba, *J. Phys. Soc. Jpn.*, 2015, **84**, 044706.

14 K. Chen, C. D. Paola, B. Du, R. Zhang, S. Laricchia, N. Bonini, C. Weber, I. Abrahams, H. Yan and M. Reece, *J. Mater. Chem. C*, 2018, **6**, 8546.
15 K. Chen, B. Du, N. Bonini, C. Weber, H. Yan and M. J. Reece, *J. Phys. Chem. C*, 2016, **120**, 27135.
16 J. H. Pi, G. E. Lee, I. H. Kim, *J. Electron Mater.*, 2019, DOI: 10.1007/s11664-019-07710-9
17 N. Tsujii and T. Mori, *Appl. Phys. Express*, 2013, **6**, 043001.
18 R. Ang, A. Ullah Khan, N. Tsujii, K. Takai, R. Nakamura, and T. Mori, *Angew. Chem. Int. Ed.*, 2015, **54**, 12909.
19 A. U. Khan, R. A. R. A. Orabi, A. Pakdel, J-B. Vaney, B. Fontaine, R. Gautier, J-F. Halet, S. Mitani, and T. Mori, *Chem. Mater.* 2017, **29**, 2988.
20 R-z. Zhang, K. Chen, B. Du, and M. J. Reece, *J. Mater. Chem. A*, 2017, **5**, 5013.
21 A. Pfitzner and S. Reiser, *Z. Kristallogr.*, 2002, **217**, 51.
22 A. Pfitzner and T. Bernert, *Z. Kristallogr.*, 2004, **219**, 20.
23 B. Xu, X. Zhang, Y. Sun, J. Zhang, Y. Wang, and L. Yi, *J. Phys. Soc. Jpn.*, 2014, **83**, 094606.
24 K. Suekuni, Y. Shimizu, E. Nishibori, H. Kasai, H. Saito, D. Yoshimoto, K. Hashikuni, Y. Bouyrie, R. Chetty, M. Ohta, E. Guilmeau, T. Takabatake, K. Watanabe, and M. Ohtaki, *J. Mater. Chem. A*, 2019, **7**, 228.
25 E. J. Skoug, J. D. Cain, D. T. Morelli, M. Kirkham, P. Majsztrik, and E. Lara-Curzio, *J. Appl. Phys.*, 2011, **110**, 023501.
26 E. J. Skoug, J. D. Cain, and D. T. Morelli, *Appl. Phys. Lett.*, 2011, **98**, 261911.
27 F. Izumi and K. Momma, *Solid State Phenom.*, 2007, **130**, 15.
28 R. D. Shannon, Acta Cryst., 1976, **A32**, 751.
29 V. I. Fistul, *Heavily Doped Semiconductors*, Plenum, New York, 1969.

Co-substitution of Ge and P for Sb in Cu_3SbS_4 famatinite boosted dimensionless thermoelectric figure of merit.